A RETURN-TO-ISOTROPY LANGEVIN SUBGRID-SCALE DISPERSED PHASE MODEL FOR LARGE-EDDY SIMULATIONS OF BUBBLE-LADEN FLOWS

Fang-yu Chen
Department of Engineering Mechanics
Tsinghua University
100084 Beijing, China
chen-fy20@mails.tsinghua.edu.cn

Chun-Xiao Xu
Department of Engineering Mechanics
Tsinghua University
100084 Beijing, China
xucx@tsinghua.edu.cn

Wei-Xi Huang
Department of Engineering Mechanics
Tsinghua University
100084 Beijing, China
hwx@tsinghua.edu.cn

ABSTRACT

Bubble-laden flows are prevalent in both natural and industrial applications. In this study, a new return-to-isotropy Langevin-type model is proposed for the large-eddy simulation of bubble-laden turbulence. Simulations are conducted in downward vertical bubble-laden turbulent channel flows with a friction Reynolds number of $Re_\tau = 590$. The new Langevin model improves the prediction of bubble velocity statistics, yielding results that are closer to direct numerical simulation than those obtained with the other two subgrid-scale models: Approximate deconvolution method (ADM) and the stochastic Langevin models of Knorps & Pozorski (2021). Moreover, it reduces the anisotropy of the fluid Reynolds stress tensor at bubble locations. Finally, the influence of the model parameter C_R is examined, and an approximate estimation formula is proposed to determine C_R automatically.

INTRODUCTION

Bubble-laden turbulent flows occur widely in both natural and industrial contexts, such as air entrainment at the ocean surface and bubble-induced drag reduction on ships. Most Euler-Lagrange studies to date have employed direct numerical simulation (DNS) for the fluid phase, while relatively few have applied large-eddy simulation (LES) (Breuer & Hoppe, 2017). In LES, only the large turbulent scales are resolved, while the subgrid-scale (SGS) motions are modeled. However, these unresolved SGS motions significantly affect the dynamics of the dispersed phase and cannot be neglected (Marchioli, 2017). To address this issue, numerous SGS models for dispersed phases (particles and bubbles) have been proposed, including approximate deconvolution models (ADM) (Stolz et al., 2001) and stochastic Langevin models (Fede & Simonin, 2006). ADM approximates an inverse filter operator to reconstruct the SGS velocity. Langevin models introduce an additional SGS velocity or directly modify the full velocity, thereby increasing particle kinetic energy (Knorps & Pozorski, 2021). In contrast, it is well established that in single-phase LES (particularly on coarse grids), the streamwise Reynolds stress is typically overestimated, while the wall-normal and spanwise components are underestimated, due to SGS modeling errors (Kravchenko & Moin, 1997). The application of Langevin models further amplifies the streamwise bubble Reynolds stress and increases its anisotropy, pushing the predictions farther from DNS results. The motivation of the present study is to propose a new Langevin SGS model that reduces anisotropy and improves the prediction of bubble velocity statistics.

PARAMETER SETTINGS

In this study, downward vertical bubble-laden turbulent channel flows are simulated using both DNS and LES. The computational domain is illustrated in figure 1. The domain size is $2\pi h \times 2h \times \pi h$, with channel half-width $h = 0.08$ m. All simulations are driven by a constant pressure gradient of $\mathrm{d}P_0/\mathrm{d}x = 0.68\,Pa/m$, corresponding to a friction Reynolds number of $Re_\tau = 590$. Since the main objective is the development of a new SGS model for the bubble phase, all cases are one-way coupled; bubble feedback to the carrier flow is neglected.

For both DNS and LES, the streamwise and spanwise directions are discretized using uniform grids, while the wall-normal direction is discretized using stretched grids. As shown in Table 1, the DNS case uses $512 \times 320 \times 384$ mesh grid points. For LES, three grids are considered: a fine grid ($128 \times 128 \times 128$, M1), a medium grid ($96 \times 128 \times 96$, M2), and a coarse grid ($64 \times 128 \times 96$, M3). The wall-normal resolution is kept sufficiently fine for wall-resolved LES (Choi & Moin, 2012).

As shown in Table 2, three bubble diameter cases are considered, $d = [110, 160, 220]\,\mu$m, corresponding to

Table 1. Grid parameters for DNS and three cases of LES.

Type	Resolution	Δx^+	Δz^+	$\Delta y^+_{\min}$
DNS	$512\times320\times384$	7.2	4.8	0.04
M1	$128\times128\times128$	29.0	14.5	0.4
M2	$96\times128\times96$	38.6	19.3	0.4
M3	$64\times128\times96$	59.0	19.3	0.4

normalized diameters $d^+ = [0.8, 1.2, 1.6]$. The selected bubbles are smaller than or comparable to the Kolmogorov microscale η^+; therefore, they are treated as point particles, and finite-size corrections (e.g., Faxén and undisturbed-velocity corrections) are neglected (Balachandar & Liu, 2023). For all cases, $Eo = O(10^{-3}) \ll 1$, indicating non-deformable bubbles (Clift, R. et al., 1978). The Froude number is fixed at $Fr = 0.0083 \ll 1$, implying strong buoyancy effects and appreciable mean slip (Mathai et al., 2020). Although $St \in [0.018, 0.073] \ll 1$, the ratio $St/Fr = O(1)$ indicates that gravitational crossing-trajectory effects remain important for bubble transport (Mathai et al., 2016).

Table 2. Bubble parameters for three diameter cases.

d (μm)	d^+	$\tilde{t}_b$ (ms)	St	St/Fr	Eo
110	0.8	0.34	0.018	0.89	0.0016
160	1.2	0.71	0.039	1.89	0.0034
220	1.6	1.35	0.073	3.57	0.0065

FLUID AND BUBBLE MODELING

For LES, the filtered incompressible Navier-Stokes equations are solved using a second-order finite-difference method (Kim et al., 2002), with the subgrid-scale stress modeled using the dynamic Smagorinsky model (Germano et al., 1991). The governing equations are:

$$\frac{\partial \overline{u}_i}{\partial x_i} = 0 \tag{1}$$

$$\frac{\partial \overline{u}_i}{\partial t} + \overline{u}_j \frac{\partial \overline{u}_i}{\partial x_j} = -\frac{1}{\rho_f}\frac{\partial \overline{p}}{\partial x_i} + \nu \frac{\partial^2 \overline{u}_i}{\partial x_j \partial x_j} + \frac{1}{\rho_f}\frac{dP_0}{dx}\delta_{1,i} + \frac{\partial \tau_{ij}}{\partial x_j} \tag{2}$$

where $\overline{u}_i$ and $\overline{p}$ are the filtered velocity and pressure. The subgrid-scale stress τ_{ij} is modeled using the eddy-viscosity approach: $\tau^d_{ij} = 2\nu_t \overline{S}_{ij}$, where $\overline{S}_{ij} = \frac{1}{2}(\partial \overline{u}_i/\partial x_j + \partial \overline{u}_j/\partial x_i)$ is the resolved strain-rate tensor and $\nu_t = (C_S\Delta)^2\sqrt{2\overline{S}_{ij}\overline{S}_{ij}}$ is the SGS viscosity with dynamic coefficient C_S determined via the Germano identity.

The Lagrange method is employed to track bubbles individually. The bubble equation of motion is given by (Maxey & Riley, 1983):

$$\begin{aligned}\frac{\mathrm{d}\boldsymbol{u}_b}{\mathrm{d}t} &= \left(1 - \frac{\rho_f}{\rho_b}\right)\boldsymbol{g} + C_D\frac{3}{4d}\frac{\rho_f}{\rho_b}|\boldsymbol{u}_s|(-\boldsymbol{u}_s) + \frac{\rho_f}{\rho_b}\frac{\mathrm{D}\boldsymbol{u}_{@b}}{\mathrm{D}t} \\ &+ C_L\frac{\rho_f}{\rho_b}(-\boldsymbol{u}_s)\times(\nabla\times\boldsymbol{u})_{@b} + C_W\frac{\rho_f}{\rho_b}\frac{2}{d}|u_{sw}|^2\hat{\boldsymbol{e}}_y \\ &+ C_M\frac{\rho_f}{\rho_b}\left(\frac{\mathrm{D}\boldsymbol{u}_{@b}}{\mathrm{D}t} - \frac{\mathrm{d}\boldsymbol{u}_b}{\mathrm{d}t}\right) - C_B\int_{-\infty}^{t} K_B(t-\tau)\frac{\mathrm{d}\boldsymbol{u}_s}{\mathrm{d}t}\mathrm{d}\tau\end{aligned} \tag{3}$$

where $\boldsymbol{u}_s = \boldsymbol{u}_b - \boldsymbol{u}_{@b}$ is the bubble slip velocity, and $\boldsymbol{u}_{@b}$ is the fluid velocity at the bubble location. The terms on the right-hand side of (3) represent, in order, the buoyancy/gravity force, drag force, pressure gradient force, lift force, wall-lift force, added mass force, and Basset history force.

In DNS, $\boldsymbol{u}_{@b}$ is obtained directly by interpolation. In LES, in contrast, $\boldsymbol{u}_{@b}$ is decomposed into two parts: the resolved fluid velocity at the bubble location, $\overline{\boldsymbol{u}}_{@b}$, and the subgrid-scale (SGS) velocity, $\boldsymbol{u}_{sg}$. The resolved component $\overline{\boldsymbol{u}}_{@b}$ is still obtained by interpolation of the filtered velocity field, whereas the SGS component $\boldsymbol{u}_{sg}$ must be modeled.

Two widely used dispersed-phase SGS models are evaluated: the approximate deconvolution model (ADM) (Stolz et al., 2001) and the stochastic Langevin model (Knorps & Pozorski, 2021).

ADM reconstructs the unfiltered velocity $\bar{u}_i + u_{sg,i}$ through approximate inversion of the filter operator G via a series expansion of the filter operator inverse Q_N (Stolz et al., 2001). For the approximate unfiltered velocity u_i^*, the approximate inverse can be written as

$$\begin{aligned}\bar{u}_i + u_{sg,i} &\approx u_i^* = \mathrm{Q}_N * \bar{u}_i \\ &= \bar{u}_i + (\bar{u}_i - \bar{\bar{u}}_i) + (\bar{u}_i - 2\bar{\bar{u}}_i + \bar{\bar{\bar{u}}}_i) + \cdots\end{aligned} \tag{4}$$

where

$$\mathrm{Q}_N = \sum_{\nu=0}^{N}(\mathrm{I}-\mathrm{G})^{\nu} \approx \mathrm{G}^{-1}, \quad \text{if } |\mathrm{I}-\mathrm{G}| < 1, \tag{5}$$

and the subgrid velocity is obtained as $u_{sg,i} = u_i^* - \bar{u}_i$. In the present work, $N = 3$ is used, which can provide a good balance between accuracy and computational cost. However, ADM is limited to homogeneous turbulence and its accuracy deteriorates rapidly in wall-bounded flows (Marchioli, 2017).

The stochastic modeling of fluid velocity originates from the classical Langevin equation for Brownian motion. In turbulence modeling, this concept was fundamentally advanced by the Generalized Langevin Model (GLM) (Pope, 1985), which represents the unclosed fluctuating pressure-gradient and viscous-dissipation effects as a continuous stochastic process. This approach was subsequently extended to large-eddy simulation (LES) to model the unresolved subgrid-scale (SGS) velocity seen by dispersed particles (Fede & Simonin, 2006). Building on these foundations, Knorps & Pozorski (2021) extended the stochastic framework to inhomogeneous, wall-bounded turbulence (here referred to as the LKP model), which explicitly incorporates the anisotropy and cross-correlations of the SGS fluid velocity:

$$\mathrm{d}u_{sg,i} = \left(-\frac{u_{sg,i}}{\tau^*_{sg,i}} - u_{sg,j}\frac{\partial \overline{u}_i}{\partial x_j} + \frac{\partial \tau_{ij}}{\partial x_j}\right)\mathrm{d}t + \sqrt{\frac{2\sigma_i^2}{\tau^*_{sg,i}}}\mathrm{d}W_i \quad (6)$$

where $\mathrm{d}W_i$ is the Wiener increment, σ_i is the SGS velocity scale in direction i, and $\tau^*_{sg,i}$ is the SGS memory-decay time scale. To account for crossing-trajectory effects caused by bubble-fluid slip, the directional time scales are corrected as $\tau^*_{sg,1} = \tau_{sg}\left(1+\beta^2 u_s^2/(2k_{sg}/3)\right)^{-1/2}$ and $\tau^*_{sg,2} = \tau^*_{sg,3} = \tau_{sg}\left(1+4\beta^2 u_s^2/(2k_{sg}/3)\right)^{-1/2}$, where $\beta = 0.2$. The SGS turbulent kinetic energy is evaluated as $k_{sg} = C_I \Delta^2 |\overline{S}|^2$, and the coefficient C_I is obtained from a Germano-identity-based dynamic procedure. The SGS velocity scale σ_i is computed with a scale-similarity dynamic strategy analogous to that for k_{sg}, but in a directional form, so the modeled SGS intensity is anisotropic rather than isotropic.

A RETURN-TO-ISOTROPY LANGEVIN MODEL

As demonstrated in the subsequent section, both the ADM and LKP models tend to amplify the bubble Reynolds stresses in all three directions. In contrast to a balanced enhancement, this effect disproportionately amplifies the streamwise component, thereby exacerbating the anisotropy of the bubble Reynolds stress. To address this limitation, a new return-to-isotropy Langevin (LRI) model is proposed.

The LRI model is inspired by the return-to-isotropy concept of Rotta (1951) in Reynolds-stress transport theory, where the pressure-rate-of-strain term is formulated to be directly proportional to the normalized anisotropy tensor, actively driving anisotropic turbulence back toward an isotropic state. Adapting this principle to the present SGS-velocity framework, the key idea is to introduce a directionally selective damping mechanism when the LES resolved field exhibits excessive streamwise anisotropy. The SGS velocity evolution equation is thus modified to:

$$\begin{aligned}\mathrm{d}u_{sg,i} = &\left(-\frac{u_{sg,i}}{\tau^*_{sg,i}}\left[1 + C_R b^*_{ii}\mathrm{sgn}\left(u_{sg,i}u'_{@b,i}\right)\right]\right. \\ &\left. - u_{sg,j}\frac{\partial \overline{u}_i}{\partial x_j} + \frac{\partial \tau_{ij}}{\partial x_j}\right)\mathrm{d}t + \sqrt{\frac{2\sigma_i^2}{\tau^*_{sg,i}}}\mathrm{d}W_i, \end{aligned} \quad (7)$$

where $u'_{@b,i} = u_{@b,i} - \langle u_i \rangle$ is the fluid velocity fluctuation evaluated at the bubble location, and no summation is implied for the repeated index i in equation (7). The corresponding normalized anisotropy tensor of fluid Reynolds-stress at the bubble location is defined as:

$$b^*_{ij} = \frac{u'_{@b,i}u'_{@b,j}}{u'_{@b,k}u'_{@b,k}} - \tfrac{1}{3}\delta_{ij}. \quad (8)$$

C_R is a model parameter, which will be discussed later. Compared to the baseline LKP model, the newly introduced factor $\left[1 + C_R b^*_{ii}\mathrm{sgn}(u_{sg,i}u'_{@b,i})\right]$ modifies the Langevin damping rate in a direction-aware manner. Specifically, when the streamwise fluctuation is overestimated ($b^*_{11} > 0$), an alignment in sign between $u_{sg,1}$ and $u'_{@b,1}$ enhances the damping effect, whereas opposite signs attenuate it. Consequently, this correction preferentially dissipates excessive streamwise SGS kinetic energy, driving the fluid velocity fluctuations experienced by the bubbles toward a more isotropic state.

RESULTS AND DISCUSSION

In LES, the approximate deconvolution model (ADM), Langevin model of Knorps & Pozorski (2021) (LKP), and the new return-to-isotropy Langevin model (LRI) are tested and compared with the results of LES without an SGS model and DNS.

Taking the case of $d^+ = 1.2$ bubbles on the medium mesh (M2) as an example (shown in Figure 2), both the lift force and wall-lift force in the downward vertical channel flow drive bubbles away from the wall, resulting in a preferential concentration in high-speed regions near the wall ($y^+ = 8$). LES tends to exaggerate this preference, whereas the new LRI model reduces it, yielding results that are closer to those of DNS.

As shown in figure 3, for $d^+ = 1.2$ bubbles on the medium grid, the mean bubble velocity $\langle u_b \rangle^+$ obtained from LES without an SGS model is elevated in the near-wall region ($y^+ < 10$) relative to DNS, which further proves that the preference is exaggerated. The inclusion of the ADM and LKP models produces little improvement, as the mean velocity profile remains nearly unchanged. In contrast, the new LRI model with $C_R = 1$ significantly reduces $\langle u_b \rangle^+$, yielding a close agreement with DNS.

As for the bubble Reynolds stress, due to SGS modeling errors in the LES (Kravchenko & Moin, 1997), LES without an SGS model overpredicts the streamwise Reynolds stress $\langle u'_b u'_b \rangle^+$, while underpredicting $\langle v'_b v'_b \rangle^+$ and $\langle w'_b w'_b \rangle^+$. The ADM slightly increases all three components of bubble Reynolds stress, while they are significantly increased by the LKP model. In figure 3(b), the LKP model causes $\langle u'_b u'_b \rangle^+$ to be overestimated. By contrast, the introduction of the LRI model significantly reduces $\langle u'_b u'_b \rangle^+$ in the near-wall region, aligning much more closely with DNS.

Figure 4 presents the Lumley triangle at bubble locations to quantify turbulence anisotropy (Lumley & Newman, 1977). The normalized anisotropy tensor of bubble Reynolds stress is defined as

$$b_{ij} = \frac{\langle u'_{b,i}u'_{b,j} \rangle}{\langle u'_{b,k}u'_{b,k} \rangle} - \frac{1}{3}\delta_{ij}. \quad (9)$$

Its second and third invariants are

$$\mathrm{II}_b = -\frac{1}{2}b_{ij}b_{ji}, \quad \mathrm{III}_b = \frac{1}{3}b_{ij}b_{jk}b_{ki}. \quad (10)$$

In the III_b–II_b plane, the LES trajectory without an SGS model shifts toward the one-component side, indicating excessive streamwise anisotropy. ADM produces only marginal change, and LKP tends to further strengthen anisotropy. By contrast, the LRI model moves the trajectory toward the DNS curve and toward the isotropic state, showing clear anisotropy recovery.

The influence of the model parameter C_R is examined in figure 5 for three bubble diameters and three grid resolutions. $\Delta\langle u'_{@b}u'_{@b}\rangle_p^{**}$ for the LRI model is defined as $\Delta\langle u'_{@b}u'_{@b}\rangle_p^{**} = \Delta\langle u'_{@b}u'_{@b}\rangle_p^{*}\sqrt{1+\beta^2 u_s^2/\sigma_1^2}$, where $\Delta\langle u'_{@b}u'_{@b}\rangle_p^{*} = \left(\frac{\langle u'_{@b}u'_{@b}\rangle\big|_{\mathrm{LKP}} - \langle u'_{@b}u'_{@b}\rangle\big|_{\mathrm{LRI}}}{\langle u'u'\rangle\big|_{\mathrm{LES}}}\right)\Bigg|_{y_p}$ is the normalized difference of $\langle u'_{@b}u'_{@b}\rangle$ between LKP and LRI at $y_p^+ = 15$ (peak height of fluid streamwise Reynolds stress), where $\langle u'u'\rangle = \langle \overline{u}'\overline{u}'\rangle + \sigma_1^2$ is the fluid full velocity Reynolds stress in LES. The factor $\sqrt{1+\beta^2 u_s^2/\sigma_1^2}$ accounts for crossing-trajectory effects, with $\beta = 0.2$.

Results show that $\Delta\langle u'_{@b}u'_{@b}\rangle_p^{**}$ exhibits an excellent linear correlation with C_R, approximately following $\Delta\langle u'_{@b}u'_{@b}\rangle_p^{**} \approx 0.2C_R$. Since the bubble inertia is minimal, the increment of $\langle u'_{@b}u'_{@b}\rangle$ between LKP and DNS at $y_p^+ = 15$ can be approximated by the increment of $\langle u'u'\rangle$ between LES and DNS, $\Delta\langle u'_{@b}u'_{@b}\rangle\big|_{y_p,\mathrm{LKP}} \approx \Delta\langle u'u'\rangle\big|_{y_p,\mathrm{LES}}$. Based on this relationship, the parameter C_R is estimated to reduce $\langle u'_{@b}u'_{@b}\rangle$ in the LRI model at y_p to match DNS. The resulting estimation formula is:

$$C_R \approx \alpha\sqrt{1+\beta^2 u_s^2/\sigma_1^2}\,\Delta\langle u'u'\rangle^*\big|_{y_p,\mathrm{LES}} \tag{11}$$

where $\Delta\langle u'u'\rangle^*\big|_{y_p,\mathrm{LES}} = \left(\frac{\langle u'u'\rangle\big|_{\mathrm{LES}} - \langle u'u'\rangle\big|_{\mathrm{DNS}}}{\langle u'u'\rangle\big|_{\mathrm{LES}}}\right)\Bigg|_{y_p}$ is the normalized difference of streamwise Reynolds stress at $y_p^+ = 15$. Moreover, $\alpha = 5$ and $\beta = 0.2$ are chosen under the present conditions.

CONCLUSION

A new return-to-isotropy Langevin-type model is proposed for the large-eddy simulation of bubble-laden turbulent flow, based on the Langevin model of Knorps & Pozorski (2021). Simulations are performed for downward vertical channel flows. The new Langevin model reduces both the mean bubble velocity and the streamwise bubble Reynolds stress, yielding results that are significantly closer to direct numerical simulation compared with other subgrid-scale models. In LES without an SGS model, the anisotropy of the fluid Reynolds stress tensor at bubble locations is amplified relative to DNS, whereas the new model effectively reduces this anisotropy. Moreover, the normalized reduction of the fluid Reynolds stress at bubble locations exhibits a nearly linear correlation with the model parameter C_R, enabling the formulation of an estimation equation for C_R.

REFERENCES

Balachandar, S. & Liu, Kai 2023 A correction procedure for self-induced velocity of a finite-sized particle in two-way coupled Euler–Lagrange simulations. International Journal of Multiphase Flow 159, 104316.

Breuer, M. & Hoppe, F. 2017 Influence of a cost–efficient Langevin subgrid-scale model on the dispersed phase of large–eddy simulations of turbulent bubble–laden and particle–laden flows. International Journal of Multiphase Flow 89, 23–44.

Choi, Haecheon & Moin, Parviz 2012 Grid-point requirements for large eddy simulation: Chapman's estimates revisited. Physics of Fluids 24 (1), 011702.

Clift, R., Grace, J.R. & Weber, M.E. 1978 Bubbles, Drops, and Particles. London: Whole. Academic Press.

Fede, Pascal & Simonin, Olivier 2006 Numerical study of the subgrid fluid turbulence effects on the statistics of heavy colliding particles. Physics of Fluids 18 (4), 045103.

Germano, Massimo, Piomelli, Ugo, Moin, Parviz & Cabot, William H. 1991 A dynamic subgrid-scale eddy viscosity model. Physics of Fluids A: Fluid Dynamics 3 (7), 1760–1765.

Kim, Kyoungyoun, Baek, Seung-Jin & Sung, Hyung Jin 2002 An implicit velocity decoupling procedure for the incompressible Navier–Stokes equations. Numerical Methods in Fluids 38 (2), 125–138.

Knorps, Maria & Pozorski, Jacek 2021 Stochastic modeling for subgrid-scale particle dispersion in large-eddy simulation of inhomogeneous turbulence. Physics of Fluids 33 (4), 043323.

Kravchenko, A.G. & Moin, P. 1997 On the Effect of Numerical Errors in Large Eddy Simulations of Turbulent Flows. Journal of Computational Physics 131 (2), 310–322.

Lumley, John L. & Newman, Gary R. 1977 The return to isotropy of homogeneous turbulence. J. Fluid Mech. 82 (1), 161–178.

Marchioli, Cristian 2017 Large-eddy simulation of turbulent dispersed flows: A review of modelling approaches. Acta Mech 228 (3), 741–771.

Mathai, Varghese, Calzavarini, Enrico, Brons, Jon, Sun, Chao & Lohse, Detlef 2016 Microbubbles and microparticles are not faithful tracers of turbulent acceleration. Phys. Rev. Lett. 117 (2), 024501.

Mathai, Varghese, Lohse, Detlef & Sun, Chao 2020 Bubbly and Buoyant Particle–Laden Turbulent Flows. Annu. Rev. Condens. Matter Phys. 11 (1), 529–559.

Maxey, Martin R. & Riley, James J. 1983 Equation of motion for a small rigid sphere in a nonuniform flow. Physics of Fluids 26 (4), 883–889.

Pope, S.B. 1985 PDF methods for turbulent reactive flows. Progress in Energy and Combustion Science 11 (2), 119–192.

Rotta, J. 1951 Statistische Theorie nichthomogener Turbulenz. Z. Physik 131 (1), 51–77.

Stolz, S., Adams, N. A. & Kleiser, L. 2001 An approximate deconvolution model for large-eddy simulation with application to incompressible wall-bounded flows. Physics of Fluids 13 (4), 997–1015.

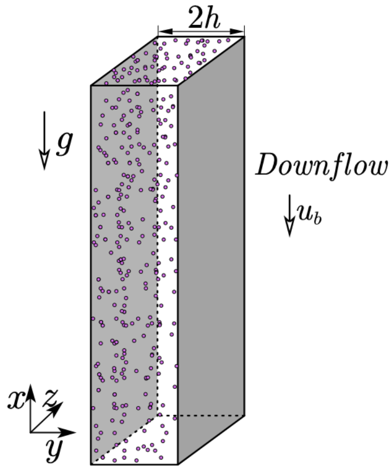

Figure 1. Diagram of computational setup

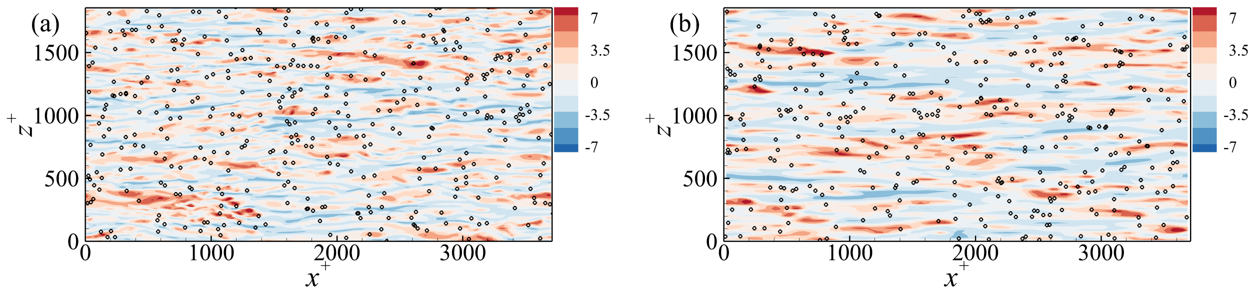

Figure 2. Instantaneous fluid velocity fluctuations and bubble distribution at $y^+ = 8$: (a) LES without an SGS model; (b) LES with return-to-isotropy Langevin model, $C_R = 1$.

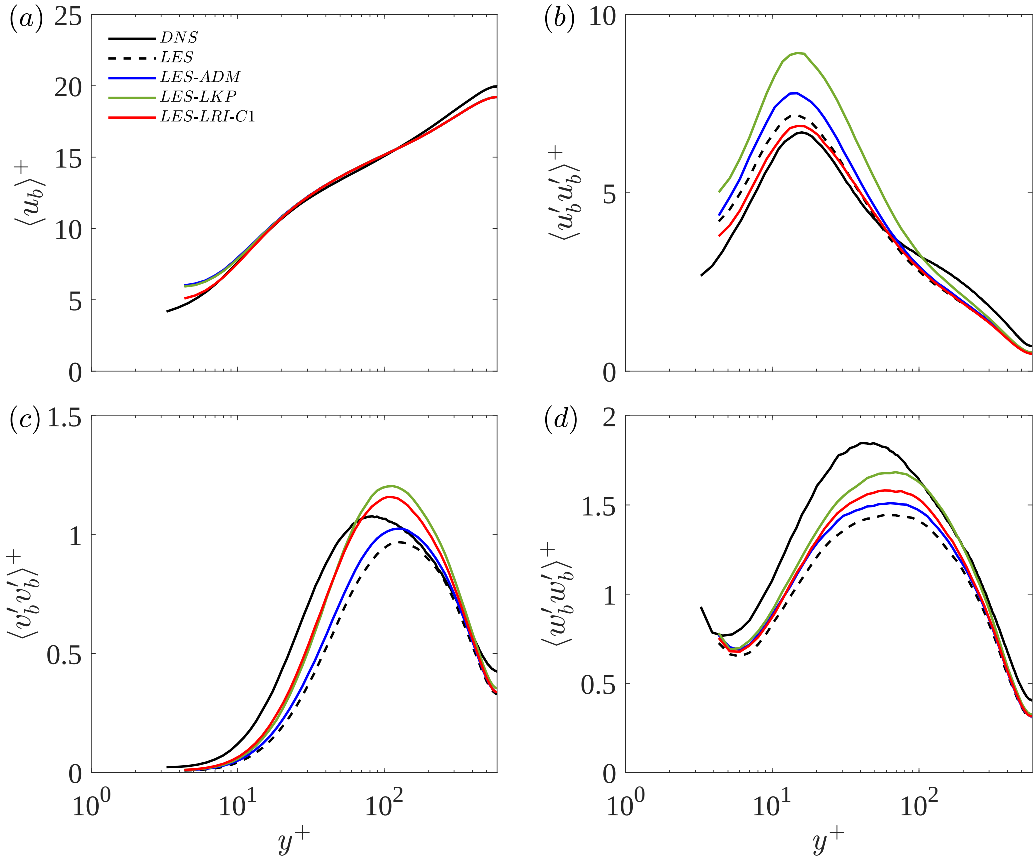

Figure 3. Bubble velocity statistics: (a) Mean bubble velocity; (b-d) Bubble Reynolds stresses. DNS: DNS results; LES: LES without an SGS model; LES-ADM: LES with approximate deconvolution model (ADM); LES-LPK: LES with Langevin model of Knorps & Pozorski (2021); LES-LRI-C1: LES with the return-to-isotropy Langevin model, $C_R = 1$.

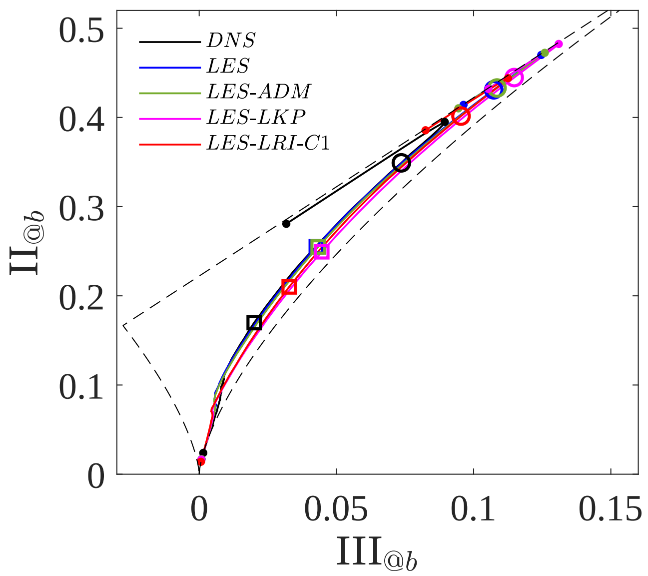

Figure 4. Invariant map of the anisotropy tensor b_{ij}. Lines: trajectory across the channel; dots: endpoints and turning points of the lines; circles: at $y^+ = 15$; squares: at $y^+ = 40$.

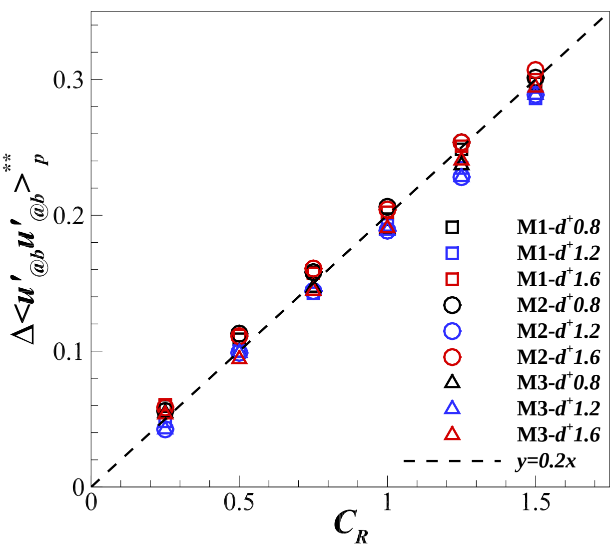

Figure 5. Relationship between $\Delta\langle u'_{@b}u'_{@b}\rangle_p^{**}$ at $y_p^+ = 15$ and model parameter C_R.